Evaluation of TRMM multi-satellite precipitation analysis (TMPA) in a mountainous region of the central Andes range with a Mediterranean climate

Lina Mabel Castro, Marcelo Miranda and Bonifacio Fernández

ABSTRACT

Estimating the spatial variability of precipitation for hydrological purposes is a challenge, especially in mountainous regions with sparse rain gauges. This study assessed the use of the satellite product Tropical Rainfall Measuring Mission Multi-satellite Precipitation Analysis (TMPA) for the rainfall estimation at the local and regional level, on a daily and monthly basis. The evaluation was carried out in a mountainous region of the central Andes Range with a Mediterranean climate. The performance of the satellite estimation was carried out using categorical metrics, residual methods, and correlation and efficiency measures. The local analysis showed that TMPA product performance was better for rainfall events of medium magnitude. Regional analysis results suggest that TMPA products are able to capture the mean spatial pattern for flat areas on a monthly basis. However, the intercomparison in the mountains is likely not reliable, because there are not enough rain gauges to enable a spatial comparison in this area. The satellite estimates also tend to miss precipitation that is enhanced by flow lifting over the mountains. Moreover, the low performance is because the precipitation in the study site is predominantly produced by frontal mechanisms, where the ice content is also lower than that from convective origin.

Key words | categorical evaluation, Mediterranean region, mountainous regions, sparse rain gauges, TMPA

Lina Mabel Castro (corresponding author)
Bonifacio Fernández
Departamento de Ingeniería Hidráulica y
    Ambiental,
Pontificia Universidad Católica de Chile,
Av. Vicuña Mackenna 4860,
Santiago,
Chile
E-mail: lecastro@uc.cl

Lina Mabel Castro
Centro de Investigación para la Gestión Integrada
    de Desastres Naturales (CIGIDEN),
Chile

Marcelo Miranda
Departamento de Ecosistemas y Medio Ambiente,
de la Pontificia Universidad Católica de Chile,
Chile

INTRODUCTION

Precipitation is the primary component of the hydrologic cycle, and the physical result of the global atmospheric circulation influenced by local biophysical conditions (Michaelides *et al.* 2009). Precipitation is also an important meteorological variable, and is a key factor in hydrology, climatology, meteorology, and agronomy, among other fields. Geometric, statistical, and geo-statistical methods have been developed and applied to estimate precipitation spatially (Thiessen 1911; Tabios & Salas 1985; Daly *et al.* 1994; Thornton *et al.* 1997; Ninyerola *et al.* 2000; Marquínez *et al.* 2003; Kurtzman *et al.* 2009; Zhang & Srinivasan 2009, 2010; Ashiq *et al.* 2010; Teegavarapu *et al.* 2012). However, the effectiveness of these methods is susceptible to the number of rain gauges available in the study area and the

frequency of the analyses. Globally, many countries have limited numbers of rain gauges, and they are sparsely distributed, making it difficult to capture the spatio-temporal variability of rainfall. This situation becomes even more complex in mountainous areas where the magnitude and spatial distribution of precipitation is affected by the distinct geographic features present. According to Viviroli *et al.* (2007), at least 50% of mountainous regions, totaling 25% of the Earth's surface, play an essential or supporting role for downstream regions. Establishing the magnitude and spatial distribution of precipitation is a challenge in itself for a variety of reasons. Capturing the spatio-temporal variability of precipitation due to orographic characteristics, the types of storms (i.e. convective, frontal), event intermittence,

and the discontinuity inherent in the spatial distribution of rainfall events is quite complex (Barros & Lettenmaier 1994; Hewitson & Crane 2005; Buytaert *et al.* 2006). One potential solution to the scarcity of rain gauges is gathering data using remote sensors. Compared to traditional rain gauges, satellite observations offer an acceptable representation of the temporal and spatial distribution of precipitation (Petty 1995; Collischonn *et al.* 2008; Scheel *et al.* 2011; Ward *et al.* 2011; Li *et al.* 2012, 2013).

Towards the end of the 1990s, a program called Tropical Rainfall Measuring Mission (TRMM) was launched as a joint project between NASA (National Aeronautics and Space Administration) and the Japanese space agency, JAXA (Japan Aerospace Exploration Agency). The program's primary goal is to increase knowledge about global water and energy cycles by capturing images of tropical rainfall (Adler *et al.* 2007; Huffman *et al.* 2007). As algorithms have improved over the years, many satellites have been launched and new methods for measuring precipitation have been introduced. The most important of these are the Tropical Rainfall Measuring Mission Multi-satellite Precipitation Analysis (TMPA) products, which have (50°S–50°N) coverage almost across the entire globe.

TMPA provides a calibration-based sequential scheme for combining precipitation estimates from multiple satellites, as well as gauge analyses where feasible, with the goal that the final product will have a calibration traceable back to the single 'best' satellite estimate (Huffman *et al.* 2007). TMPA depends on input from two different sets of sensors. The first set is composed of a Microwave Imager (TMI) on TRMM, Special Sensor Microwave Imager (SSM/I) on Defense Meteorological Satellite Program (DMSP) satellites, Advanced Microwave Scanning Radiometer-Earth Observing System (AMSR-E) on Aqua, and the Advanced Microwave Sounding Unit-B (AMSU-B) on the National Oceanic and Atmospheric Administration's (NOAA) satellite series. The second set of sensors consists of infrared (IR) data collected by the international constellation of geosynchronous Earth orbit satellites. However, TMPA also makes use of additional sources, including (i) TMI and the TRMM precipitation radar (PR) and (ii) monthly rain gauge analysis developed by Global Precipitation Climatology Program (GPCP). With these data, it is possible to calibrate precipitation estimates and limit the

bias of land-based gauge analyses. TMPA estimates are produced in four stages: (i) microwave precipitation estimates are calibrated and combined; (ii) infrared precipitation estimates are created using calibrated microwave precipitation; (iii) microwave and IR estimates are combined; and (iv) rain gauge data are incorporated (Huffman *et al.* 2007). The data are compiled using three different time intervals: every three hours (3B42), daily (3B42 derived), and monthly (3B43), all with a spatial resolution of $0.25° \times 0.25°$.

Given the availability of rainfall data obtained by remote sensors, it is necessary to examine and assess the estimations made with them and compare them with the data recorded by the rain gauge networks. Studies published that evaluate TMPA products generally fall into two groups. The first type consists of studies that compare satellite estimations and data recorded by rain gauges or large-scale global precipitation datasets (Collischonn *et al.* 2008; Su *et al.* 2008; Hand & Shepherd 2009; Javanmard *et al.* 2010; Scheel *et al.* 2011; Li *et al.* 2012, 2013). Most of these studies analyze large basin regions on a monthly basis. The second type of study is based on the incorporation of satellite precipitation data within large-scale hydrologic models. This approach also evaluates and compares data through classic hydrologic simulation methods (Harris *et al.* 2007; Collischonn *et al.* 2008; Behrangi *et al.* 2010; Li *et al.* 2012, 2013). Data assessment has largely been carried out using distributed and lumped hydrologic models on large-scale basins, where the scale of spatial modeling has been larger or equal to the scale at which the satellite information is generated.

Like many mountainous countries, Chile has a limited number of rain gauges. Most of these gauges are located in valleys and very few are situated in mountainous or foothill areas. However, mountainous regions require more attention during rainfall monitoring because there is greater precipitation in these areas. Mountainous regions also have a greater impact on downstream water resources that are often used for drinking water, agriculture, and hydropower. This situation is even more significant in regions with a Mediterranean climate, where precipitation is greater in the fall and winter seasons. Satellite data offer an alternative source for collecting information on rainfall. This could help researchers obtain data in areas with limited accessibility, and where the lack of rain gauges is a hindrance to the spatial estimation of precipitation. The quality of

satellite-based data on precipitation has not been verified in mountainous regions with a Mediterranean climate, which is precisely the profile of the Andes Range in central Chile. It is therefore necessary to carry out an assessment to identify potential TMPA products that could accurately estimate precipitation in regions with a Mediterranean climate where there are also strong orographic influences. In our research, an evaluation was done at the local and regional level, on a daily and monthly basis. Local analysis was carried out comparing TMPA estimates with the precipitation recorded by rain gauges. The ability of satellite products to capture occurrence/non-occurrence of precipitation events was evaluated on a daily basis. Numerical evaluation on both a local and regional scale was made on a daily and monthly basis.

This paper is structured as follows. The 'Data and methods' section presents a description of the study site, rain gauges, and satellite data employed. It also includes a description of the categorical and numerical metrics used

in assessing the ability to capture precipitation and the performance of the TMPA estimates. Additionally, this section provides a short description of the interpolation method employed in the regional analysis. The results and discussion then follow. The final section of the paper contains a summary and provides the main conclusions.

DATA AND METHODS

Study site

The Bio Bio Region is located in the center of southern Chile, between latitudes $36°15'$ S and $38°24'$ S and longitudes $71°07'$ W and $73°34'$ W. The basin has a total area of $36,000 \text{ km}^2$ (Figure 1). The main features of the terrain include the Andes Range to the east, an intermediate depression, and the Coastal Range and adjacent coastal platform to the west (Garreaud & Rutlland 1997). The altitude
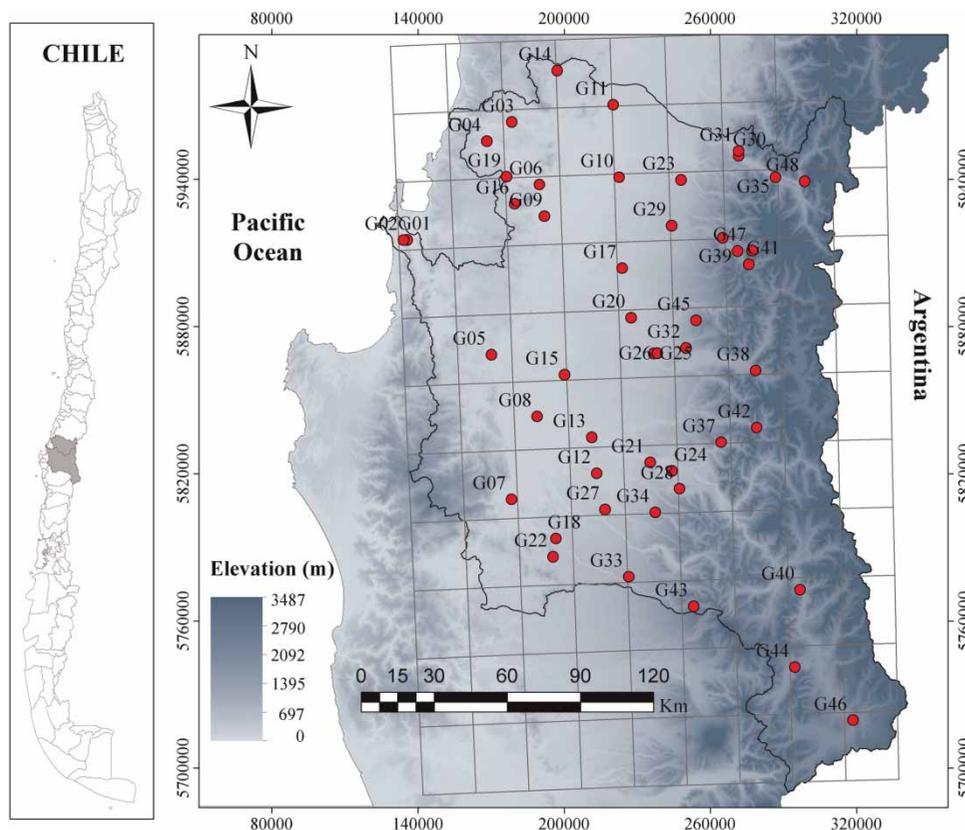

Figure 1 | Topographic representation based on the digital elevation model (STRM 90 m). The points denote rain gauges in the Bio Bio Region, and the grey grid TMPA grid cells.

ranges from 0 to 3,500 m. The climate of this region reflects the transition from a Mediterranean climate to a mild, humid climate. In the low areas, moderate temperatures are maintained throughout the year. Spring and summer (October through March) are mostly dry, while fall and winter (April through September) are more humid, cloudy, rainy, and cold (Instituto Geográfico Militar 1985). Eighty-five percent of the annual precipitation occurs in winter. The region's primary form of terrain is the Andes Mountain Range. The presence of this mountain chain produces a wide spectrum of microclimates and types of precipitation (Garreaud 2009), and causes complex spatial rainfall patterns. Annual precipitation (around 1,100 mm) is quite uniform between the coast and the foothills of the Andes Range, but increases to more than 2,000 mm in the Andes. According to Viale & Nuñez (2010), precipitation in the study site is predominantly produced by frontal mechanisms. These frontal mechanisms are largely (~80%) brought about by cold fronts, with a few cases (~20%) corresponding to cut-off lows, post-cold-fronts, and warm front synoptic situations.

Rain gauges and satellite products

This evaluation was carried out with daily rainfall data collected over 5 years (from January 1, 2005 through December 31, 2009). In the Bio Bio Region, there are 48 rain gauges managed by Dirección General de Aguas (DGA – Chile). These are placed at a range of elevations, from 5 m to 1,430 m, with one station located every 750 km^2 (Figure 1 and Table 1). The rain gauges are mostly located in the Central Valley (36 out of 48 gauges), at elevations between 0 and 700 m. However, since the maximum elevation within the study region is 3,500 m, a large part of this region does not have any gauges. Table 1 shows the mean daily rainfall (mm d^{-1}), the maximum daily rainfall (mm d^{-1}), and the percentage of days with no rainfall for each rain gauge in the evaluation period. The precipitation in general tends to increase with elevation, but for the higher rain gauges tends to decrease (Figure 2). This situation is contrary to what would be expected for these altitudes (Barry 1992), but can be explained by the poor quality of data recorded by the gauges in these higher areas due to the presence of snow. It is worth noting that in addition to the poor quality

of the data recorded by the gauge, the overall scarcity of gauges at high altitudes has hindered the characterization of spatial patterns of precipitation within the study site (Falvey & Garreaud 2007). Recordings of zero precipitation are frequent since 80% of rainfall occurs during the winter (June to August), with few precipitation events during spring and summer. This is characteristic of Mediterranean climates. However, the rainfall recorded by the rain gauges has high dispersion, with daily maximums equivalent to between 10 and 20% of annual precipitation (Table 1).

The satellite image dataset used in this study consisted of 3-hourly 3B42 products on a 0.25° × 0.25° latitude-longitude grid (TMPA 3B42). The satellite information is free and can be downloaded from NASA's web page (http://mirador.gsfc.nasa.gov/cgi-bin/mirador/collectionlist.pl?keyword=TRMM_3B42) in ASCII file format. Individual files can be downloaded as well as a list of the image URLs. A total of 14,600 images or ASCII files were downloaded for the evaluation period, using the URL list and an automatic file download program (http://gnuwin32.sourceforge.net/packages/wget.htm). It was necessary to accumulate 3-hourly TMPA estimates from 12UTC (coordinated universal time) until 9UTC of the following day in order to find the daily precipitation. This method guaranteed that the daily precipitation estimated by the TMPA would correspond to the same time period as the precipitation recorded by the gauges (8 am to 8 am of the following day). To this end, a sub-routine was developed on Matlab® to manage the 14,600 images and to aggregate data on a daily and monthly basis. Local evaluation identified the cells that included at least one gauge (Figure 1). If there was more than one gauge in the cell, the TMPA estimate in each cell was compared with the average precipitation recorded by those gauges.

Data analysis

The assessment of the TMPA products was carried out taking into account two approaches: Local Analysis and Regional Analysis. The first consists of a comparison of the precipitation recorded in the rain gauges and the TMPA estimates for those cells where the gauges were found (Figure 1). The second consists of a comparison between all of the data sources detailing the average precipitation for three areas: the entire region (Region), central valley (Valley) and

Table 1 │ Basic metrics about the available rain gauges for the study period January 1, 2005 through December 31, 2009

		Rain gauges					Rain gauges		
ID	Name	Pmean	Pmax.	%Zeros	ID	Name	Pmean	Pmax.	%Zeros
G1	Rio biobio en desembocadura	2.05	70.3	74.2	G25	Rio laja en tucapel	2.74	152.3	73.6
G2	Concepcion DGA	3.29	108	75.9	G26	Tucapel	4.14	148.7	75.6
G3	San agustin de puñual	2.54	164	81.6	G27	Pilguen	4.93	125.5	70.8
G4	Coelemu	2.51	133	84.0	G28	Cerro el padre	5.37	122	75.5
G5	Laja	3.25	52.5	71.0	G29	Mayulermo	4.02	113.5	83.4
G6	Nueva aldea	2.77	135	86.7	G30	Rio ñuble	4.38	124.8	75.5
G7	Angol	3.30	130.6	74.4	G31	San fabian	4.17	160	83.8
G8	Los angeles	3.02	111	76.6	G32	Trupan	4.65	119	74.2
G9	Chillancito	2.94	192.5	77.0	G33	Encimar malleco	5.21	85	76.4
G10	Chillan viejo	2.77	112	81.5	G34	Poco a poco	6.89	153	74.7
G11	Millauquen	2.57	120	78.4	G35	Caracol	6.14	167	80.7
G12	Mulchen	3.62	112.6	72.7	G36	Diguillin	5.82	150	80.1
G13	San carlos de puren	3.31	180	77.4	G37	Quillaileo	6.08	127	73.6
G14	Mangarral	2.29	145.2	85.5	G38	Abanico	5.80	110	73.2
G15	Las achiras	2.66	64.5	78.6	G39	Fundo atacalco	6.04	140	79.5
G16	Cancha los litres	2.47	187.5	83.2	G40	Rio bio-bio en llanquen	4.47	115.8	56.6
G17	Pemuco	3.28	137	84.9	G41	San lorenzo	5.92	134	81.2
G18	Collipulli	3.70	80	72.5	G42	San lorenzo en bio-bio	5.52	125	75.1
G19	Rafael	3.25	62	81.8	G43	Laguna malleco	7.26	132	71.2
G20	Cholguan	3.53	180	78.2	G44	Lonquimay	3.88	102	74.7
G21	Quilaco	3.82	105.2	72.7	G45	Las cruces	4.90	158	76.7
G22	Ercilla (vida nueva)	3.74	80	70.1	G46	Liucura	2.64	75	83.2
G23	Coihueco embalse	3.80	108	81.9	G47	Las trancas	5.17	123	84.0
G24	Rio biobio en rucalhue	3.53	113.3	48.5	G48	Caman	6.12	169.3	80.4

P mean: mean daily rainfall (mm d^{-1}), *P* max.: maximum daily rainfall (mm d^{-1}), %Zeros: percentage of zero-rain days in the evaluation period.
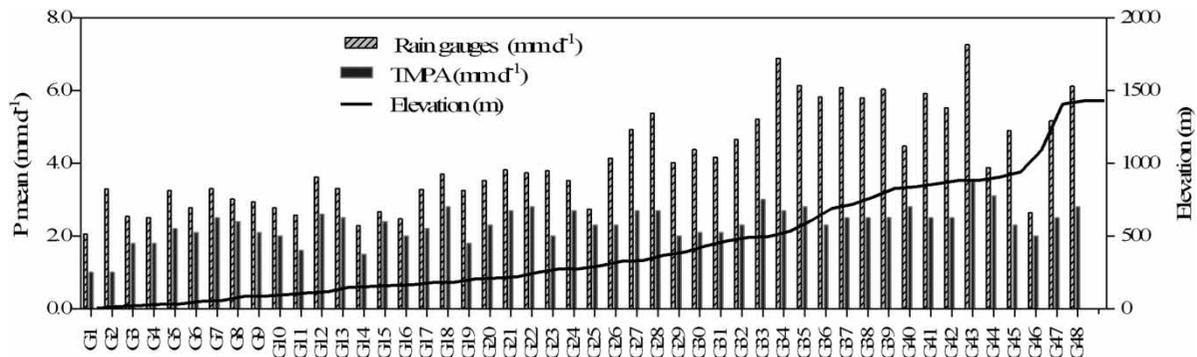

Figure 2 │ Daily mean rainfall (mm d^{-1}) obtained based on data from the rain gauges and the TMPA estimates. The rain gauges are sorted by elevation.

mountainous zone (Cordillera). In order to quantify the performance of the TMPA products for the local and regional analysis on a daily and monthly basis, the following statistical and interpolation methods were used.

Statistical evaluation

In the Local Analysis, categorical and numerical metrics were used to evaluate the TMPA products on a daily basis (Legates & McCabe 1999; Bennett *et al.* 2013). Categorical metrics were computed in order to verify the frequency of the correct and incorrect TMPA estimates. Numerical metrics were used to measure the magnitude of the error in terms of residuals, correlation, and efficiency. The categorical metrics evaluated the occurrence of precipitation in a binary manner (Yes/No) by using a contingency table (Table 2), which made it possible to calculate several categorical metrics, including: accuracy, bias score, probability of detection, false alarm ratio (FAR), and index of success, among others (see Bennett *et al.* (2013) for a more detailed explanation). In this analysis, the FAR and the probability of detection (POD) were used. The former measures the fraction of rain detections in the TMPA rain estimates that were actually false alarms, $FAR = b/(a + b)$, and the latter quantifies the fraction of rain events which were correctly estimated by TMPA in relation to the total amount of rain events measured, $POD = a/(a + c)$. For FAR and POD metrics, scores range from 0 to 1, with a perfect score of 1 in POD and a perfect score of 0 in FAR.

In order to establish a level of confidence in the TMPA estimates, we used residual metrics, correlation, and efficiency measures. Bias and Mean Absolute Error (MAE) were used as residual metrics. Bias is simply the mean of the residual,

Table 2 | Standard structure of a contingency table

		Observed Events	
		Yes	No
TMPA estimates	Yes	Hits[a]	False alarms[b]
	No	Misses[c]	Correct rejections[d]

[a]The number of hits (rain is estimated and it is observed).
[b]The number of false alarms (rain is estimated but it is not observed).
[c]The number of misses (rain is not estimated but it is observed).
[d]The correct number of rejections (rain is not estimated and it is not observed).
Adapted from Bennett *et al.* (2013).

indicating whether the TMPA tends to under- or over-estimate the observed rainfall, with an ideal value of zero (Equation (1)). However, positive and negative errors tend to cancel each other out. To avoid such cancellation and to measure the magnitude of error in absolute terms, we used MAE (Equation (2)), penalizing the higher errors (Bennett *et al.* 2013). The ability of TMPA estimates to maintain the same pattern of recorded rainfall was tested with the Pearson Product Moment Correlation measure (PPMC) and the Nash–Sutcliffe coefficient of efficiency (NSE). PPMC measures the linear correlation between the observed and estimated rainfall, and its value lies between −1 and 1 (Equation (3)). NSE indicates how well the TMPA explains the variance of the observations (Equation (4)). NSE = 1 indicates a perfect estimation, while NSE < 0 implies that the TMPA estimates are worse than simply using the mean (Bennett *et al.* 2013).

$$\text{Bias}_j = \frac{1}{N} \sum_{i=1}^{N} \left(P^j_{\text{est},i} - P^j_{\text{obs},i} \right) \qquad (1)$$

$$\text{MAE}_j = \frac{1}{N} \sum_{i=1}^{N} \left| P^j_{\text{est},i} - P^j_{\text{obs},i} \right| \qquad (2)$$

$$\text{NSE}_j = 1 - \frac{\sum_{i=1}^{N} \left(P^j_{\text{est},i} - P^j_{\text{obs},i} \right)^2}{\sum_{i=1}^{N} \left(P^j_{\text{obs},i} - \overline{P^j_{\text{obs}}} \right)^2} \qquad (3)$$

$$\text{PPMC}_j = \frac{\text{Cov}\left(P^j_{\text{est},i}, P^j_{\text{obs},i} \right)}{\sigma^j_{\text{est},i} \sigma^j_{\text{obs},i}} \qquad (4)$$

where j indicates the cell that coincides geographically with the presence of a gauge or group of gauges. $P^j_{\text{obs},i}$ is the daily rainfall observed or the average rainfall of the group of gauges within the cell. And, $P^j_{\text{est},i}$ is the rainfall estimated by the satellite product for the day i, and evaluated for the total days, N, considered in the analysis.

Spatial estimation of precipitation

In order to carry out a comparison of the average rainfall at the regional scale, it is necessary to use a spatial interpolation

method that would enable obtaining the average rainfall for each region. Geometric, statistical, and geo-statistical methods have been developed to estimate the spatial distribution of precipitation. Among the geometric methods, the most popular include the Thiessen polygons (Thiessen 1911) and the Inverse Distance Weighted (IDW) (Tabios & Salas 1985). Because of their simplicity, they have been employed at various spatial and temporal scales (Goovaerts 2000; Fortin *et al.* 2001; Yu *et al.* 2001; Buytaert *et al.* 2006; Haberlandt 2007; Serbin & Kucharik 2009; Zhang & Sriniva-san 2009; Chen *et al.* 2010; Yang *et al.* 2011; Chen & Liu 2012). These statistical methods use simple and multiple linear regressions to relate precipitation to physical predictor vari-ables such as elevation, latitude, longitude, distance from the ocean, slope orientation, etc. (Daly *et al.* 1994; Goovaerts 2000; Ninyerola *et al.* 2000; Marquínez *et al.* 2003; Guan *et al.* 2005; Kurtzman *et al.* 2009; Hwang *et al.* 2012). However, the more predictor variables that are considered by the method, the more neighbor data points are needed to arrive at an estimate (Yeasmin & Pasha 2008; Chen & Liu 2012). Finally, geo-statistical methods, such as Kriging, Co-Kriging, Kriging with External Drift, and all their variants, use the struc-ture of spatial correlation among observed data in order to estimate spatial distribution of precipitation (Tabios & Salas 1985; Das *et al.* 2008; Hofstra *et al.* 2008; Ashiq *et al.* 2010). These methods are widely used and particularly successful at spatially representing monthly and annual precipitations (Goovaerts 2000; Diodato 2005; Lloyd 2005; Ninyerola *et al.* 2007; Yang *et al.* 2011). However, it is very difficult to correctly apply these methods on a daily basis in mountainous regions where rain gauges are sparsely distributed (Buytaert *et al.* 2006; Ly *et al.* 2011). The application of these methods in the Bio Bio Region was discarded due to the sparse network of rain gauges and the high spatial variability of daily rainfall in the region. For these reasons, it was decided to use a two-step interpolation method, based on the method carried out by Hewitson & Crane (2005) and Hwang *et al.* (2012). This method considers both the spatial discontinuity of daily pre-cipitation and the significant influence of the topography on its magnitude and spatial distribution (Figure 3). The first con-cept was addressed by identifying the rainfall occurrence in each grid-cell as a function of the measurements in surround-ing rain gauges. The second concept was addressed by running linear regressions between daily precipitation and
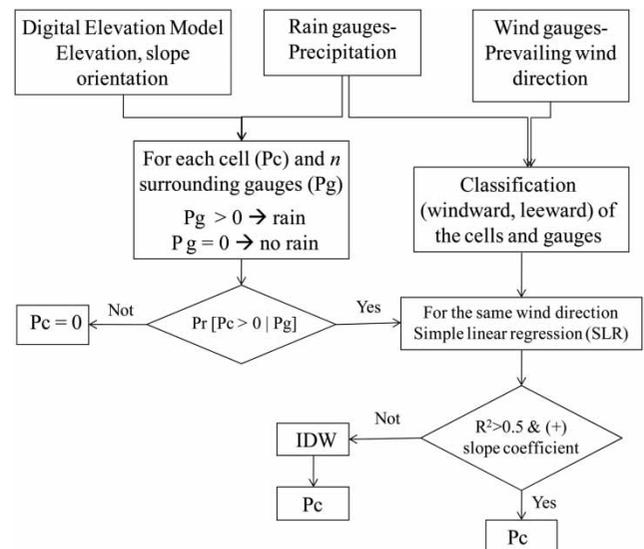

Figure 3 | Algorithm of the two-step interpolation method used to estimate spatial distribution of precipitation. Pg: precipitation recorded via rain gauge, Pc: estimated precipitation in the cell.

elevation, classified according to the slope orientation. These regressions are applied in grid-cells in which the rainfall occur-rence is identified (Castro *et al.* 2014). When it proved impossible to find an adequate regression equation, precipi-tation was estimated using IDW. After cross-validation, the interpolation method showed an underestimation bias of less than 0.16 mm d^{-1}. This value is relatively low in comparison to the mean daily precipitation of 4.3 mm d^{-1}.

RESULTS

TMPA estimates were evaluated on a daily and monthly basis from January 1, 2005 to December 31, 2009. The evalu-ation had two objectives: (1) to assess the ability of the TMPA products to capture rainfall on a daily basis (categori-cal metrics); and (2) to assess the magnitude of error in daily and monthly TMPA estimates (numerical metrics) for three spatial scales. To address the first objective, we conducted a local analysis, comparing TMPA estimates and the rainfall recorded by the gauges that were placed within the cell. To fulfill the second objective, we carried out a regional analysis, comparing the average precipitation in the basin (or part of the basin) using the TMPA grid with the mean precipitation obtained by applying an unconventional interpolation method (Figure 3).

Local analysis

Accuracy of the rain occurrence estimates was tested using categorical metrics (FAR, POD) for different rain thresholds in the evaluation period. The thresholds selected for this study varied from 0–10 mm d^{-1} (0, 2, 5, 7, 10 mm d^{-1}). A reading of 10 mm d^{-1} is approximately double the mean daily rainfall in the Bio Bio Region. Figure 4 shows the box and whisker plots, along with the temporal variation of categorical metrics assessed for different rainfall thresholds. The length of the boxes indicates the inter-quartile range, the middle line is the median and the whiskers show the 5th and 95th percentiles. Box plots were calculated monthly as an average of the categorical metrics obtained from all the rain gauges.

The upper panel of Figure 4(a) shows that rainfall events were best detected (POD > 0.5) for precipitation thresholds of less than 2 mm d^{-1}. From that threshold, the POD metric tends to decrease rapidly to values below 0.4. On the other hand, the frequency of rainfall events was overestimated (upper panel of Figure 4(b)). In general, there is a large proportion of false predictions (FAR > 0.3) relative to the total predictions made, but this tends to decrease as precipitation thresholds increase to a constant value of 0.28 (for thresholds above 4 mm d^{-1}). Figures 4(a) and 4(b) show high temporal variability of POD and FAR metrics and the impact of the assessed rainfall thresholds. Spring and summer seasons (October to March) show the highest variability for the evaluated thresholds. Rain occurrence (POD) was poorly detected in this period, with values lower than 0.2, occurring in November, December, January, and March (Figures 4(a), (c)). In the same period, the frequency of rain events was overestimated for false alarms greater than 0.7 occurring in January (Figures 4(b), (d)). The rain events were better detected in the fall and winter period, showing a decrease in variability and the same median in the box plots between thresholds. Over this period, more than 50% of rain events were detected (Figures 4(a), (c))
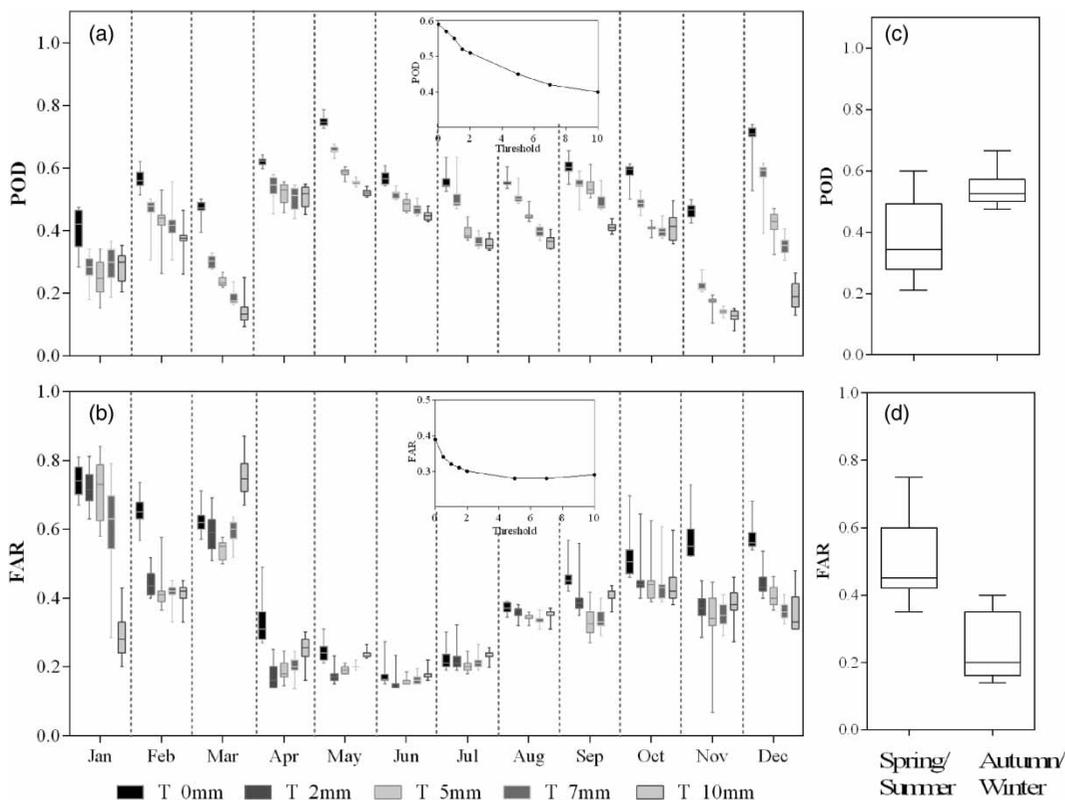

Figure 4 | Temporal distribution of POD (a) and FAR (b) metrics. These metrics were calculated for five daily precipitation thresholds (mm d^{-1}). Plots (c) and (d) show an example (threshold 2 mm d^{-1}) of the POD and FAR metrics for the spring/summer and autumn/winter periods.

and false alarm rates totaled 20% on average (Figures 4(b), (d)). The higher number of rainfall events during the rainy season, especially between May and July, explained the low FARs and the high probability of detection.

In general, TMPA estimates perform well for precipitation thresholds of less than 2 mm d^{-1}. These results are similar to those reported by Su *et al.* (2008), who evaluated the performance of TMPA daily estimates. The authors found that the agreement between TMPA estimates and the gauge product on a daily basis was best for low and medium precipitation thresholds (0.1–5 mm d^{-1}). From this value and up to 20 mm d^{-1}, the ability to capture precipitation events decreases (POD) and false alarms (FAR) increase. In our case, the same trend was obtained with the POD metric, but not with the FAR metric. In the overall assessment (upper panel of Figure 4(b)), false alarms decrease while the precipitation threshold increases to a constant value of 0.28. In the Bio Bio Region, more than 50% of rain events are less than 10 mm d^{-1}, and 30% are less than 5 mm d^{-1}. This

explains the decrease for POD and FAR metrics with increasing thresholds. Overall, there are fewer high rainfall events, and these are not being captured well by TMPA.

The scatter plots shown in Figure 5 were carried out as a graphic inspection prior to the calculation of the magnitude of error. As an example, the scatter plots for two rain gauges with their coefficient of determination (R^2) are shown in Figure 5. The diagrams show a comparison between the rain gauge records and TMPA estimates for cells located in the valley and in the mountains. In the first case, three gauges share a pixel (Figure 1); therefore, their average was used for comparison with TMPA estimates (G21-Quilaco, G24-Biobio en Rucalhue, and G34-Poco a Poco, with an average elevation of 343 m for the three gauges). In the second case, the precipitation recorded by the Abanico gauge was used for comparison with TMPA estimates in that cell (G38-Abanico gauge at an elevation of 770 m). In these examples, the diagrams show little agreement between daily, observed records and daily TMPA estimates.
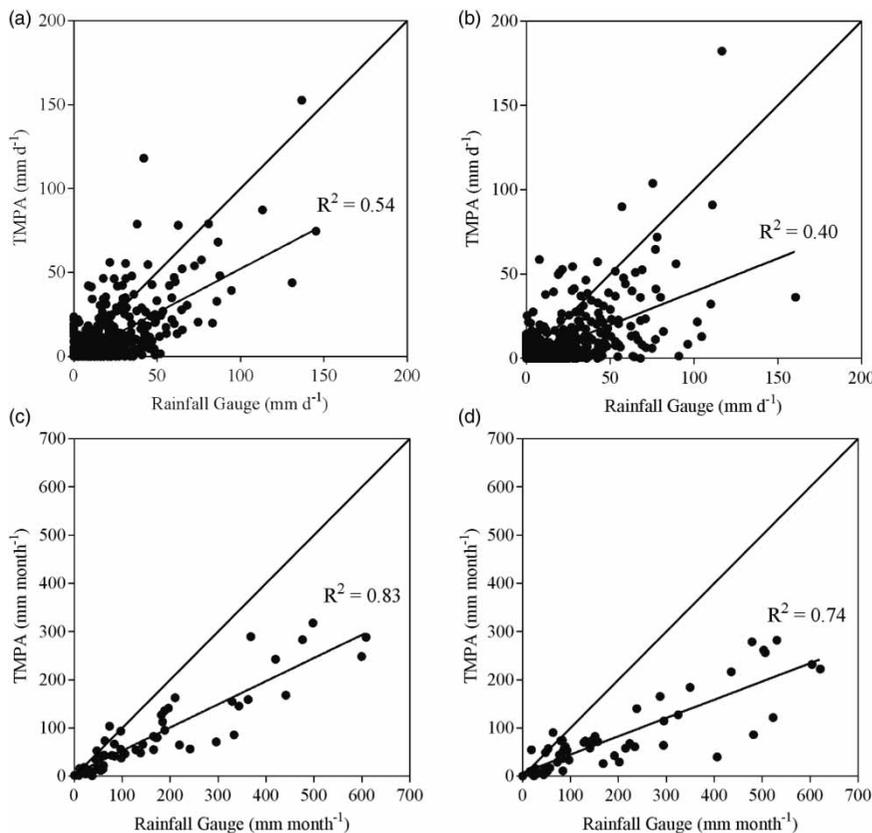

Figure 5 │ Scatterplots for TMPA estimates regarding the Quilaco (a), (c) and Abanico (b), (d) rain gauges on a daily (a), (b) and monthly (c), (d) basis.
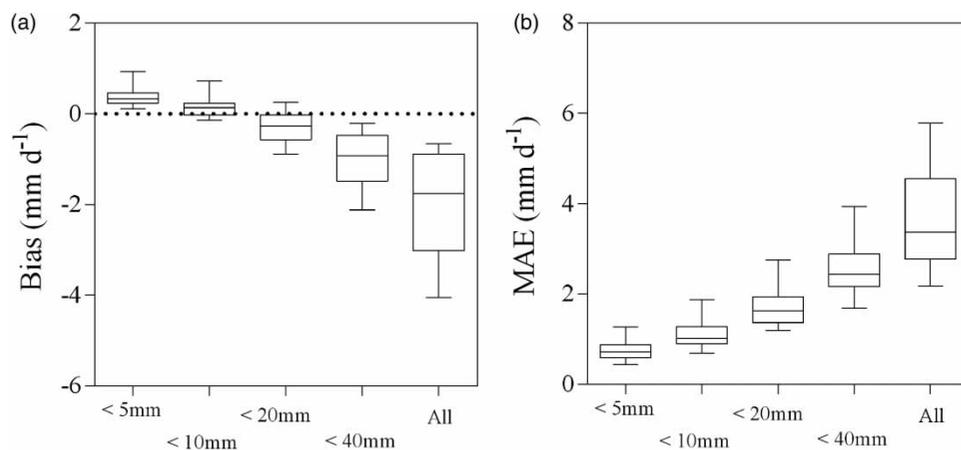
Figure 6 │ Box and whisker plots of (a) MAE (mm d⁻¹) and (b) Bias (mm d⁻¹). The box plots represent the difference between TMPA estimates and the records for rain gauges in regard to different precipitation rates. For example, the label '> 20 mm' means that the evaluation was made when the records for rain gauges were less than 20 mm. The label 'All' means that the evaluation was carried out based on all of the rain gauge records.

Figures 5(a), (b) show that the coefficient of determination was 0.54 and 0.40, respectively, for the Quilaco and Abanico gauges. In general, TMPA estimates tend to underestimate daily rainfall with few exceptions. Figure 5 (the abscissa of a and b) shows that many TMPA estimates were zero-rain, but they actually correspond to values up to 50 mm d⁻¹ and 90 mm d⁻¹ for Quilaco and Abanico. The monthly aggregation improved the agreement between the gauge records and TMPA estimates ($R^2 = 0.83$ and $R^2 = 0.74$ for Quilaco and Abanico respectively, Figure 5(c), (d)). This is because monthly accumulation eliminates daily dispersion caused by zero-rain intermittences and extreme precipitations (i.e. greater than 100 mm). On a monthly basis, the TMPA estimates represent a fair percentage of the variance of observed data, with a coefficient of determination $R^2 > 0.7$ on a monthly basis. On a daily basis, however, error increases when precipitation increases.

In order to evaluate the influence of the magnitude of rainfall on the accuracy of TMPA estimates, we defined four precipitation rates (5, 10, 20, 40 mm). We estimated the magnitude of error for each of these. Figure 6 shows the Bias and MAE for different precipitation rates on a daily basis. Both metrics show that the magnitude of error and its dispersion increases with increasing precipitation rates. However, Figure 6(a) allows us to see something additional, namely, that TMPA estimates tend to overestimate smaller rainfall events (<10 mm d⁻¹) and tend to underestimate larger events (≥10 mm d⁻¹). This situation is made clear in

Figure 7, which shows that in the most recent summer months (January, February, and March), the median for bias is near zero, and the 5th and 95th percentiles do not exceed 3 mm d⁻¹. In winter, the TMPA estimates were biased, with an interquartile range between −7.0 mm d⁻¹ and 0 mm d⁻¹. This is because the largest number of rainfall events with the highest magnitude occur during this period. Most of them are caused by cold frontal systems, resulting in orographically enhanced rain falling in the mountains.

The metrics used to assess the magnitude of error on a daily and monthly basis are depicted in box plots in Figure 8. Two of them are residual methods (Bias, MAE) and the others test the ability of TMPA estimates to preserve pattern data (PPMC, NSE). TMPA estimates strongly tend to underestimate total precipitation, with a median bias of −1.8 mm d⁻¹
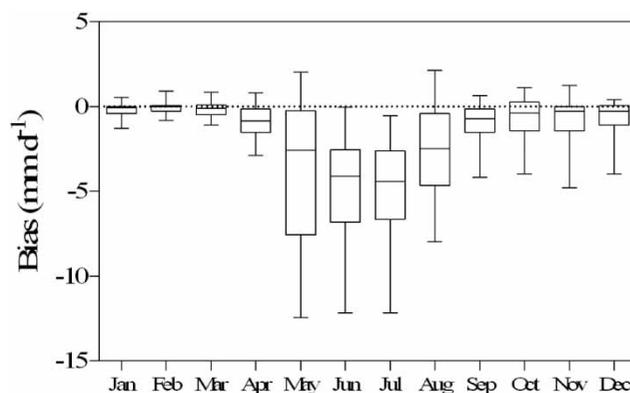

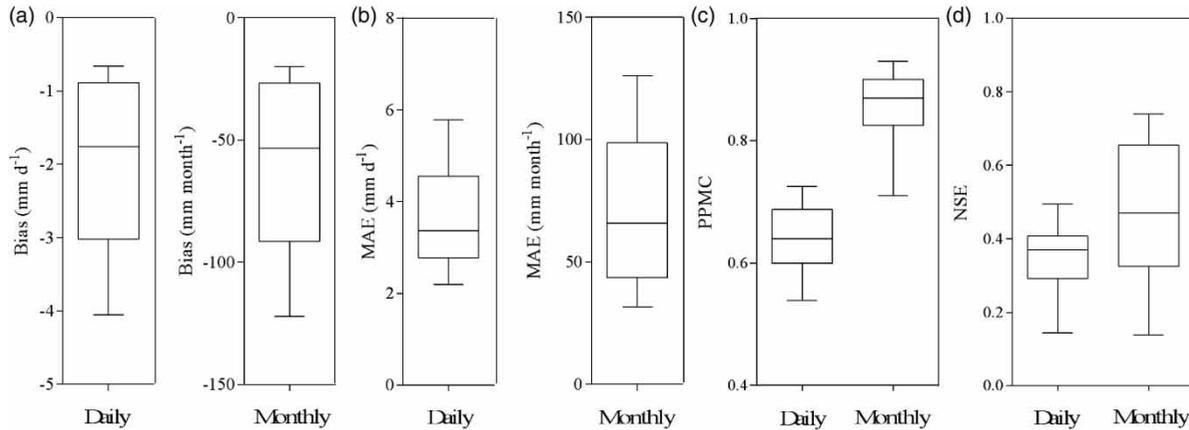**Figure 7** │ Monthly variation of daily bias.

Figure 8 | Statistical comparison of the TMPA estimates and the data from rain gauges, on daily and monthly basis for the entire evaluation period.

on a daily basis and -55 mm month^{-1} on a monthly basis. The MAE metric was of 3.5 mm d^{-1} and 53 mm month^{-1} on a daily and monthly basis, respectively. Those are high values considering that the mean daily rainfall is 4.3 mm d^{-1} and the mean monthly rainfall is 125.3 mm month^{-1}. MAE represents almost 80% of average daily precipitation on a daily basis and 42% on a monthly basis. On the other hand, correlation and efficiency performance measures show more agreement between TMPA estimates and the rain gauge records on a monthly basis (PPMC = 0.87). However, this measure only gives us an idea of the linear relationship between both sources of data. The NSE gives a better idea of the relationship between both sources, because it indicates how well the TMPA estimates explain the variance of the rain observations. On a daily basis, this measure reached a median of 0.38, and on a monthly basis the median was approximately 0.5. In local analysis, the TMPA estimates generally underestimate observations in both time scales, with worse performance measures on a daily basis. Although agreement between both sources improves on a monthly basis, the variance of rainfall observations (NSE) in the study region was only somewhat explained by TMPA estimates.

In order to assess the spatial variation of error and to define the areas for regional analysis, daily and monthly errors in each station were interpolated. Figure 9 shows the IDW interpolation of Bias, as well as PPMC and NSE measures for the entire study period. The first two measures are shown on a daily basis because the monthly spatial representation is similar. Figures 9(c), (d) show the spatial

variation for NSE on a daily and monthly basis. The differences between TMPA estimates and records from rain gauges show a clear geographic pattern, where TMPA increasingly underestimates as elevation increases. Minimum values for bias (daily) were found in the northwest in the Bio Bio Valley, and higher values were found in the mountains. In terms of correlation and efficiency measures, spatial behavior is similar to that found for bias. Linear relationships are stronger in the valley, but these tend to decrease at higher altitudes. Meanwhile, NSE tends to show more erratic behavior on a daily basis rather than on a monthly time scale. On a monthly basis, efficiency (or variance explained by TMPA estimates) reaches values higher than 0.5 in the valley, while for higher elevations, efficiency can reach values of 0.09.

Regional analysis

Regional comparison was done for the entire region, *valley*, and *cordillera*. These regions were defined based on a monthly NSE measure shown in Figure 9(d). From this interpolation, we defined the elevation from which the indicator NSE was lower than 0.5. This elevation was on average 600 m. Cells with higher elevation were classified as *cordillera*, and the cells with lower elevations were classified as *valley* (Figure 1). The average for the TMPA estimates for each region was calculated as an average of TMPA grid cells over the region. The average precipitation based on rain gauges was estimated by employing the unconventional interpolation method described in the 'Data and methods' section and in Figure 3.
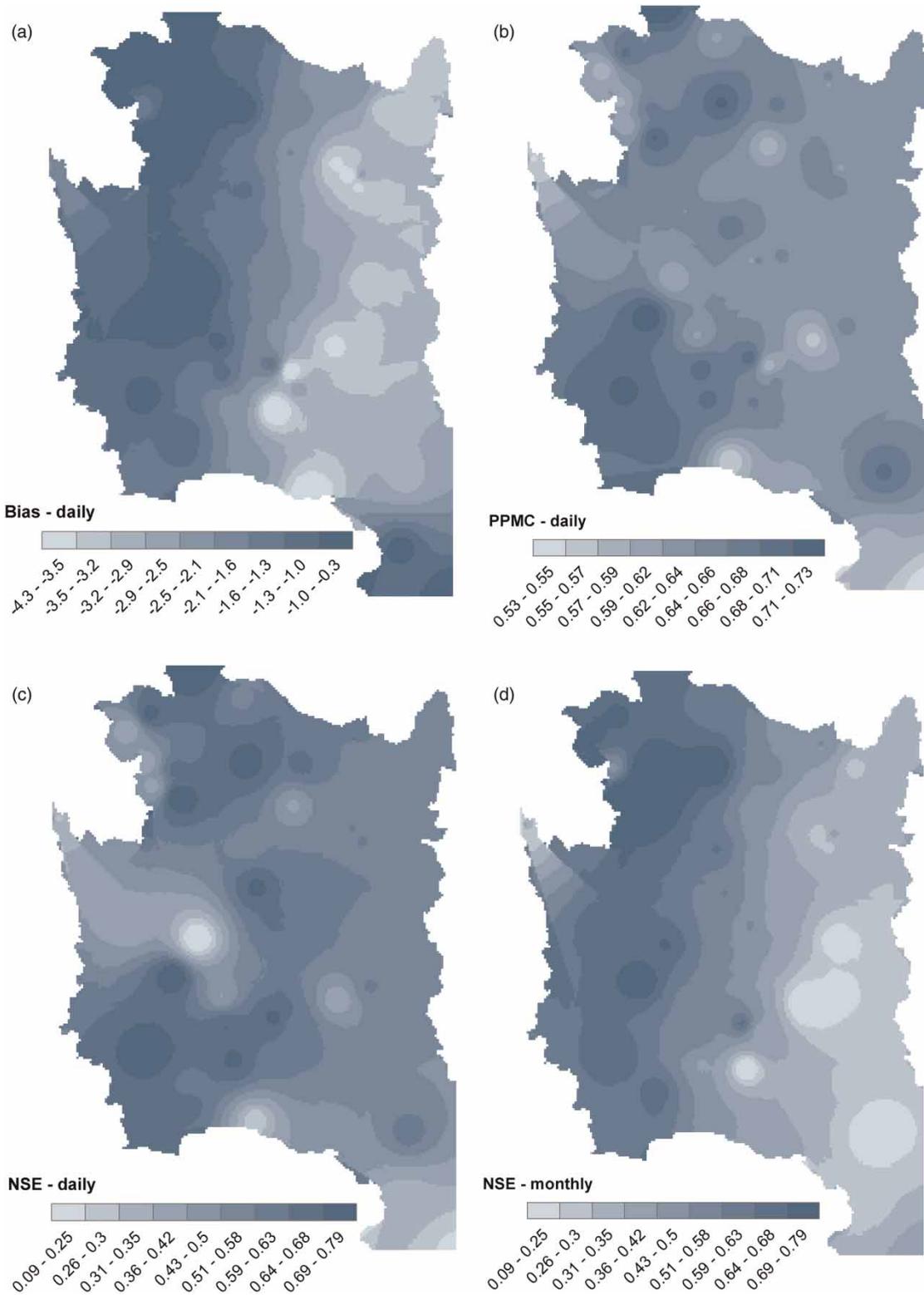
Figure 9 │ Comparison of the spatial distribution of Bias, PPMC, and NSE metrics. The interpolation method used to represent the spatial variation of these performance measures was IDW.

Figure 10 shows the scatter plots for the daily mean (by month) interpolated precipitation from rain gauges and the daily mean (by month) precipitation estimated by TMPA grid cells. Rows a, b, and c in the figure show the three areas analyzed (the entire region, *valley*, and *cordillera*), and columns 1 and 2 show the scale of time assessed. For both time scales in the three regions, TMPA underestimated the precipitation. The entire region is affected by the

error noted for the *cordillera*. On a monthly basis, the *valley* region showed more agreement between both data sources, with PPMC = 0.94 and NSE = 0.70. In contrast, the metrics for the *cordillera* show an improvement in the daily to monthly linear relationship, but the efficiency measure decreased. Although the linear relationship improves when we assess monthly correspondence, the NSE measure shows that TMPA average monthly
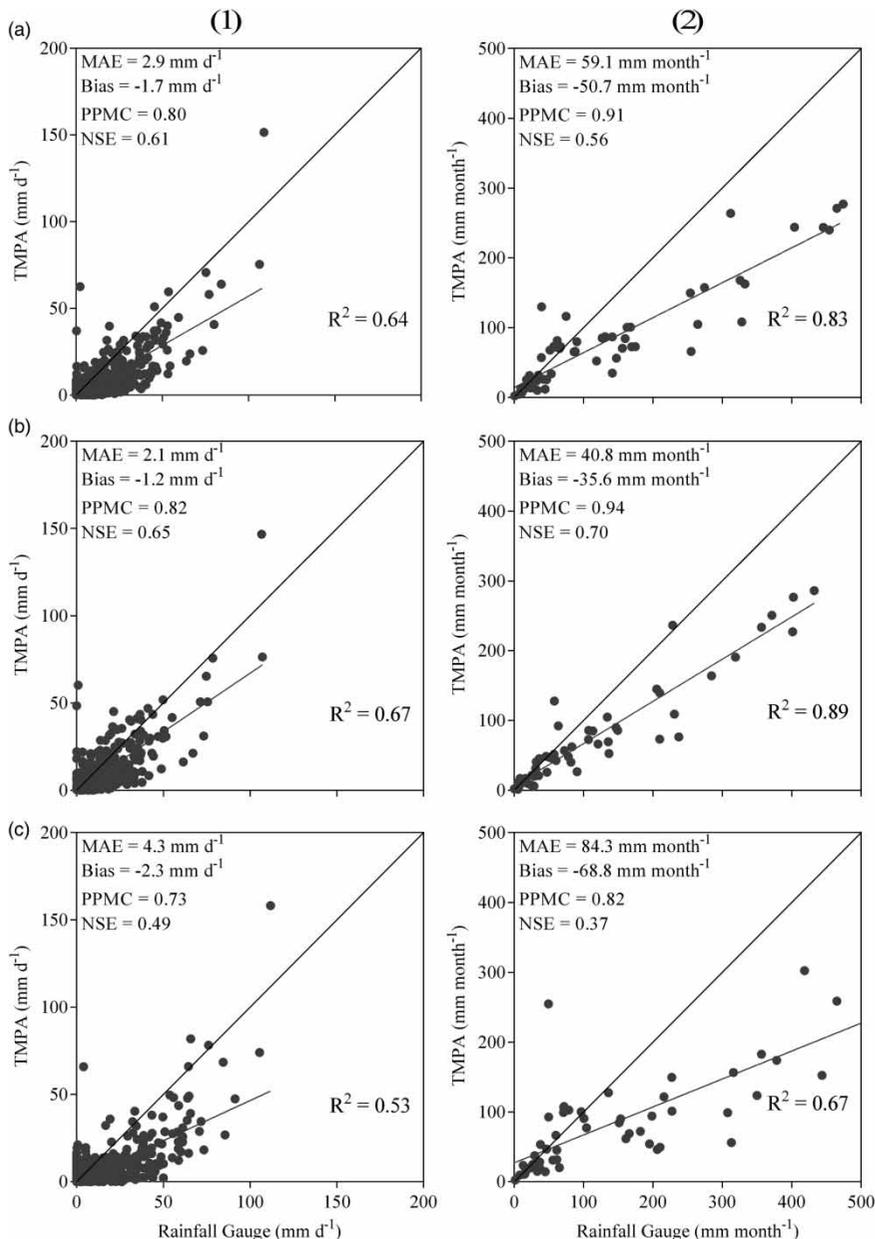

Figure 10 | Scatter plot of the average precipitation for the whole region (a), for the valley region with elevations of less than 600 m (b), and for the *cordillera* where elevations are more than 600 m (c), on daily (1) and monthly (2) bases.

precipitation does not explain the variance of average rainfall in the mountains.

DISCUSSION

Temporal assessment of categorical metrics showed that TMPA estimates in winter demonstrate agreement with the data collected by gauge, where the number of false alarms (FAR) decreases and the probability of detection (POD) increases. In winter (April to September), it is more likely that satellite algorithms detect rainfall because there is a greater frequency of rainfall events. In summer, the POD metric indicates that TMPA fails to identify precipitation events with short durations. Summer storms are spatially and temporally discontinuous, and the duration of these storms may last a few hours. This may or may not match the precipitation captured by the sensors. Satellites were not able to observe the evolution of rain events between successive 'snapshots.'

TMPA estimates underestimated the data collected by rain gauges throughout the entire study site, which were particularly biased during the winter. There are several factors that could contribute to differences between TMPA estimates and the data collected by rain gauges. Frontal episodes, characterized by widespread rainfall throughout central Chile, are the most frequent winter events. However, the magnitude of rainfall for this kind of storm is difficult to estimate with TMPA sensors. Subsequently, these data demonstrate higher dispersion and a larger negative median in the bias. Another source of error in the Bio Bio Region is the presence of the Andes Range. In both winter and summer, spatial and temporal rainfall distribution is strongly influenced by orographic effects. According to Petty (1995), the rainfall magnitude tends to be underestimated because satellite estimates tend to miss precipitation that is enhanced by flow lifting over mountains. TMPA estimates are also affected by the presence of snow. Mätzler & Standley (2000) have discussed the strong effect of the relief itself on the microwave signal, and the effect snow cover has on brightness, temperatures, and the property of polarization. The part of the Andes Range that lies within the study site is covered with snow for most of the fall, the entire winter, and most of the spring, and is characterized by a wide variety in relief.

Comparisons made between average regional rainfall, TMPA estimates, and the rain gauge records require knowledge of the magnitude and distribution of actual precipitation (Ebert *et al.* 2007). In order to produce a high quality representation of the spatial distribution of rainfall, it is necessary to have a large number of rain gauges. Since rain gauges are not equally distributed in the Bio Bio Region and are sparsely distributed in the mountains, the rain gauge analysis may be inaccurate in this region. Regional analyses show daily and monthly agreement in the valley (where the elevation is less than 600 m and where most of the rain gauges are located) with strong correlation and efficient measurements. Improvements in the performance of TMPA estimates are due to the fact that TMPA products have a spatial resolution of $0.25° \times 0.25°$. These precipitation data represent an average of what is happening in an area of 756 km^2, which is similar to the data obtained via the interpolation method. However, in the *cordillera* region no strong correlation was found between the mean precipitation estimated by TMPA data and the mean found using the unconventional interpolation method. Sparsely distributed rain gauges, their measurement error, and varied relief suggest that spatial interpolation was not valid. Thus, the intercomparison for the *cordillera* region is likely not reliable.

The behavior of both data sources, rain gauges and satellite images, is directly related to topographic and climatic characteristics of the study area. The variability in daily precipitation, highly influenced by topographic characteristics of steep slopes, peaks, and valleys, make rainfall one of the most challenging variables to estimate. In the study zone, rainfall events are strongly influenced by the relief and the Mediterranean climate (Instituto Geográfico Militar 1985; Garreaud 2009). This causes high levels of discontinuity in the daily spatial distribution of precipitation and high variability in the *cordillera* region. Gauges G21 (Quilaco, 221 m, southern orientation) and G34 (Poco a Poco, 533 m, northern orientation) are perfect examples: their radial distance is no more than 20 km (both contained in one pixel of the TMPA product), which suggests major differences in the magnitude of precipitation recorded on one winter day. The precipitation recorded in the G21 gauge is a third of the rainfall recorded in the G34 gauge.

In general, differences found in local and regional analyses are related to geographic and climatic conditions

across the study region, and to the spatial and temporal scale at which the satellite captures the data and the algorithms used to compile this information. One possible source of error includes the characteristics of clouds that produce precipitation in the study area. VIS/IR rainfall estimation schemes are most useful in estimating climatic scale distributions for largely convective rainfall with cold temperatures and ice near the cloud top (Petty 1995; Ebert *et al.* 2007). In the study zone, rainfall is caused mainly by cold fronts, where the cold air mass propagates and lifts the warmer, less dense air. The air mass that produces clouds and precipitation ahead of and along with the cold front could affect the brightness and temperature of the cloud top, which is measured by a VIS/IR sensor and has better spatial and temporal resolution than TMPA products.

SUMMARY AND CONCLUSIONS

In this paper, we evaluated the TMPA estimates in comparison with the precipitation recorded by rain gauges on a daily and monthly basis, on both a local and regional scale. The local analysis consisted of a comparison of TMPA estimates and those recorded by the rain gauges (cell vs. rain gauge). The main purpose of this analysis was to evaluate the proficiency of TMPA in capturing daily precipitation events by using categorical statistics such as the FAR and Probability of Detection. The regional analysis consisted of dividing the study region into two sections: *valley* and *cordillera*. Measurements for residual, correlation, and efficiency were used to evaluate the performance of TMPA estimates.

The local analysis carried out through categorical and numerical metrics showed that TMPA product performance was better for rainfall events of medium magnitude. For storms with larger magnitudes, the probability of detection decreased and the bias (through underestimation) increased. In the Bio Bio Region, TMPA estimates are not reliable for estimating the magnitude of large daily events caused by cold fronts, which are typically more vigorous, produce thicker clouds, and yield more intense bands of rain.

Regional analysis results suggest that TMPA products are able to capture the mean spatial pattern for flat areas on a monthly basis. In our case, this holds true for sites at elevations below 600 m. The correlation and efficiency

showed a good correspondence between the interpolation made with the unconventional two-step interpolation method, and the average rainfall estimated by the TMPA grid. Monthly aggregation eliminates the zero-rain intermittency and reduces the variability produced by large events, with better correlation and efficiency measures. These improvements were made possible because the 3B42 TMPA products are configured based on data that are calibrated monthly (3B43). Monthly multi-satellite product and gauge are combined (3B43) in order to provide the high resolution typical of satellite and the typically small bias of gauge analysis over land (Huffman *et al.* 2007).

Geographic features, strong relief, presence of snow, and solid precipitation, coupled with climatic characteristics which produce precipitation in the study area (generally the frontal), have thus far hindered the ability to accurately estimate precipitation in the Andes. Estimating precipitation for time periods of less than a month in the Bio Bio Region still remains a challenge, given the current monitoring network. However, NASA and JAXA plan to launch a new mission in 2014, the Global Precipitation Mission (GPM). This mission will consist of an international network of satellites that will provide the most updated technology for conducting global observations of rain and snow. GPM will focus on trying to improve its reliability in regard to estimates for light rain and falling snow in medium to high altitudes.

In order to use TMPA products in an operative way addressing finer-grained spatial and temporal scales ($<0.25° \times 0.25°$, on a daily basis), the following factors should be taken into consideration: merge of satellite products, the use of data from rain gauges, and the corresponding correlation with geographic features that govern the spatial and temporal variability of rainfall. This should result in improved extrapolation of TMPA estimates in regions with few rain gauges and limited accessibility.

ACKNOWLEDGEMENTS

the Dirección General de Aguas and the Dirección Meteorológica de Chile.

REFERENCES

Adler, R., Braun, S., Stocker, E. & Marius, J. 2007 *Tropical Rainfall Measuring Mission, TRMM, Senior Review Proposal*. Laboratory for Atmospheres, NASA Goddard Space Flight Centre, Greenbelt, MD, USA.

Ashiq, M., Zhao, C., Ni, J. & Akhtar, M. 2010 GIS-based high-resolution spatial interpolation of precipitation in mountain–plain areas of Upper Pakistan for regional climate change impact studies. *Theor. Appl. Climatol.* **99** (3), 239–253.

Barros, A. P. & Lettenmaier, D. P. 1994 Dynamic modeling of orographically induced precipitation. *Rev. Geophys.* **32** (3), 265–284.

Barry, R. G. 1992 *Mountain Weather and Climate*. Routledge, New York, 506 pp.

Behrangi, A., Khakbaz, B., Jaw, T. C., AghaKouchak, A., Hsu, K. & Sorooshian, S. 2010 Hydrologic evaluation of satellite precipitation products over a mid-size basin. *J. Hydrol.* **397** (3–4), 225–237.

Bennett, N. D., Croke, B. F. W., Guariso, G., Guillaume, J. H. A., Hamilton, S. H., Jakeman, A. J., Marsili-Libelli, S., Newham, L. T. H., Norton, J. P., Perrin, C., Pierce, S. A., Robson, B., Seppelt, R., Voinov, A. A., Fath, B. D. & Andreassian, V. 2013 Characterizing performance of environmental models. *Environ. Modell. Softw.* **40**, 1–20.

Buytaert, W., Celleri, R., Willems, P., Bièvre, B. D. & Wyseure, G. 2006 Spatial and temporal rainfall variability in mountainous areas: a case study from the south Ecuadorian Andes. *J. Hydrol.* **329** (3–4), 413–421.

Castro, L., Gironás, J. & Fernández, B. 2014 Spatial estimation of daily precipitation in complex relief with scarce data using terrain orientation. *J. Hydrol.* **517**, 481–492.

Chen, D. L., Ou, T. H., Gong, L. B., Xu, C. Y., Li, W. J., Ho, C. H. & Qian, W. H. 2010 Spatial interpolation of daily precipitation in China: 1951–2005. *Adv. Atmos. Sci.* **27** (6), 1221–1232.

Chen, F.-W. & Liu, C.-W. 2012 Estimation of the spatial rainfall distribution using inverse distance weighting (IDW) in the middle of Taiwan. *Paddy Water Environ.* **10** (3), 209–222.

Collischonn, B., Collischonn, W. & Tucci, C. E. M. 2008 Daily hydrological modeling in the Amazon basin using TRMM rainfall estimates. *J. Hydrol.* **360** (1–4), 207–216.

Daly, C., Neilson, R. P. & Phillips, D. L. 1994 A statistical-topographic model for mapping climatological precipitation over mountainous terrain. *J. Appl. Meteorol.* **33** (2), 140–158.

Das, T., Bárdossy, A., Zehe, E. & He, Y. 2008 Comparison of conceptual model performance using different representations of spatial variability. *J. Hydrol.* **356** (1–2), 106–118.

Diodato, N. 2005 The influence of topographic co-variables on the spatial variability of precipitation over small regions of complex terrain. *Int. J. Climatol.* **25** (3), 351–363.

Ebert, E. E., Janowiak, J. E. & Kidd, C. 2007 Comparison of near-real-time precipitation estimates from satellite observations and numerical models. *B. Am. Meteorol. Soc.* **88** (1), 47–64.

Falvey, M. & Garreaud, R. 2007 Wintertime precipitation episodes in central Chile: associated meteorological conditions and orographic influences. *J. Hydrometeorol.* **8** (2), 171–193.

Fortin, J. P., Turcotte, R., Massicotte, S., Moussa, R., Fitzback, J. & Villeneuve, J. P. 2001 Distributed watershed model compatible with remote sensing and GIS data. I: description of model. *J. Hydrol. Eng.* **6** (2), 91–99.

Garreaud, R. & Rutlland, J. 1997 Precipitación estival en Los Andes de Chile central: aspectos climatológicos. *Atmósfera* **10** (4), 191–211.

Garreaud, R. D. 2009 The Andes climate and weather. *Adv. Geosci.* **22**, 3–11.

Goovaerts, P. 2000 Geostatistical approaches for incorporating elevation into the spatial interpolation of rainfall. *J. Hydrol.* **228** (1–2), 113–129.

Guan, H., Wilson, J. L. & Makhnin, O. 2005 Geostatistical mapping of mountain precipitation incorporating autosearched effects of terrain and climatic characteristics. *J. Hydrometeorol.* **6** (6), 1018–1031.

Haberlandt, U. 2007 Geostatistical interpolation of hourly precipitation from rain gauges and radar for a large-scale extreme rainfall event. *J. Hydrol.* **332** (1–2), 144–157.

Hand, L. M. & Shepherd, J. M. 2009 An investigation of warm-season spatial rainfall variability in Oklahoma City: possible linkages to urbanization and prevailing wind. *J. Appl. Meteorol.* **48** (2), 251–269.

Harris, A., Rahman, S., Hossain, F., Yarborough, L., Bagtzoglou, A. C. & Easson, G. 2007 Satellite-based flood modeling using TRMM-based rainfall products. *Sensors* **7** (12), 3416–3427.

Hewitson, B. C. & Crane, R. G. 2005 Gridded area-averaged daily precipitation via conditional interpolation. *J. Climate.* **18** (1), 41–57.

Hofstra, N., Haylock, M., New, M., Jones, P. & Frei, C. 2008 Comparison of six methods for the interpolation of daily, European climate data. *J. Geophys. Res.* **113**, D21110.

Huffman, G. J., Bolvin, D. T., Nelkin, E. J., Wolff, D. B., Adler, R. F., Gu, G., Hong, Y., Bowman, K. P. & Stocker, E. F. 2007 The TRMM Multisatellite Precipitation Analysis (TMPA): quasi-global, multiyear, combined-sensor precipitation estimates at fine scales. *J. Hydrometeorol.* **8** (1), 38–55.

Hwang, Y., Clark, M., Rajagopalan, B. & Leavesley, G. 2012 Spatial interpolation schemes of daily precipitation for hydrologic modeling. *Stoch. Environ. Res. Risk A.* **26** (2), 295–320.

Instituto Geográfico Militar 1985 *Geografía de Chile*. Editorial IGM, Santiago de Chile, Chile, 286 pp.

Javanmard, S., Yatagai, A., Nodzu, M., BodaghJamali, J. & Kawamoto, H. 2010 Comparing high-resolution gridded precipitation data with satellite rainfall estimates of TRMM_3B42 over Iran. *Adv. Geosci.* **25**, 119–125.

Kurtzman, D., Navon, S. & Morin, E. 2009 Improving interpolation of daily precipitation for hydrologic modelling: spatial patterns of preferred interpolators. *Hydrol. Process.* **23** (23), 3281–3291.

Legates, D. R. & McCabe, G. J. 1999 Evaluating the use of "goodness-of-fit" measures in hydrologic and hydroclimatic model validation. *Water Resour. Res.* **35** (1), 233–241.

Li, L., Ngongondo, C. S., Xu, C.-Y. & Gong, L. 2013 Comparison of the global TRMM and WFD precipitation datasets in driving a large-scale hydrological model in Southern Africa. *Hydrol. Res.* 770–788.

Li, X.-H., Zhang, Q. & Xu, C.-Y. 2012 Suitability of the TRMM satellite rainfalls in driving a distributed hydrological model for water balance computations in Xinjiang catchment, Poyang lake basin. *J. Hydrol.* **426–427**, 28–38.

Lloyd, C. D. 2005 Assessing the effect of integrating elevation data into the estimation of monthly precipitation in Great Britain. *J. Hydrol.* **308** (1–4), 128–150.

Ly, S., Charles, C. & Degre, A. 2011 Geostatistical interpolation of daily rainfall at catchment scale: the use of several variogram models in the Ourthe and Ambleve catchments, Belgium. *Hydrol. Earth Syst. Sci.* **15**, 2259–2274.

Marquínez, J., Lastra, J. & García, P. 2003 Estimation models for precipitation in mountainous regions: the use of GIS and multivariate analysis. *J. Hydrol.* **270** (1–2), 1–11.

Mätzler, C. & Standley, A. 2000 Technical note: relief effects for passive microwave remote sensing. *Int. J. Remote Sens.* **21** (12), 2403–2412.

Michaelides, S., Levizzani, V., Anagnostou, E., Bauer, P., Kasparis, T. & Lane, J. 2009 Precipitation: measurement, remote sensing, climatology and modeling. *Atmos. Res.* **94** (4), 512–533.

Ninyerola, M., Pons, X. & Roure, J. M. 2000 A methodological approach of climatological modelling of air temperature and precipitation through GIS techniques. *Int. J. Climatol.* **20** (14), 1823–1841.

Ninyerola, M., Pons, X. & Roure, J. M. 2007 Monthly precipitation mapping of the Iberian Peninsula using spatial interpolation tools implemented in a Geographic Information System. *Theor. Appl. Climatol.* **89** (3–4), 195–209.

Petty, G. W. 1995 The status of satellite-based rainfall estimation over land. *Remote Sens. Environ.* **51** (1), 125–137.

Scheel, M., Rohrer, M., Huggel, C., Villar, D. S., Silvestre, E. & Huffman, G. 2011 Evaluation of TRMM Multi-satellite Precipitation Analysis (TMPA) performance in the Central Andes region and its dependency on spatial and temporal resolution. *Hydrol. Earth Syst. Sci.* **15**, 2649–2663.

Serbin, S. P. & Kucharik, C. J. 2009 Spatiotemporal mapping of temperature and precipitation for the development of a multidecadal climatic dataset for Wisconsin. *J. Appl. Meteorol.* **48** (4), 742–757.

Su, F., Hong, Y. & Lettenmaier, D. P. 2008 Evaluation of TRMM multisatellite precipitation analysis (TMPA) and its utility in hydrologic prediction in the La Plata basin. *J. Hydrometeorol.* **9** (4), 622–640.

Tabios, G. Q. & Salas, J. D. 1985 A comparative analysis of techniques for spatial interpolation of precipitation. *J. Am. Water Resour. Assoc.* **21** (3), 365–380.

Teegavarapu, R. S. V., Meskele, T. & Pathak, C. S. 2012 Geo-spatial grid-based transformations of precipitation estimates using spatial interpolation methods. *Comput. Geosci.* **40**, 28–39.

Thiessen, A. H. 1911 Precipitation averages for large areas. *Mon. Weather Rev.* **39** (7), 1082–1089.

Thornton, P. E., Running, S. W. & White, M. A. 1997 Generating surfaces of daily meteorological variables over large regions of complex terrain. *J. Hydrol.* **190** (3–4), 214–251.

Viale, M. & Nuñez, M. N. 2010 Climatology of winter orographic precipitation over the subtropical Central Andes and associated synoptic and regional characteristics. *J. Hydrometeorol.* **12** (4), 481–507.

Viviroli, D., Dürr, H. H., Messerli, B., Meybeck, M. & Weingartner, R. 2007 Mountains of the world, water towers for humanity: typology, mapping, and global significance. *Water Resour. Res.* **43** (7), W07447.

Ward, E., Buytaert, W., Peaver, L. & Wheater, H. 2011 Evaluation of precipitation products over complex mountainous terrain: a water resources perspective. *Adv. Water Resour.* **34** (10), 1222–1231.

Yang, X., Liang, Y. & Jia, S. 2011 *Study on the Rainfall Interpolation Algorithm of Distributed Hydrological Model Based on RS, Computer and Computing Technologies in Agriculture IV – 4th IFIP*. Springer Boston, Nanchang, China, pp. 700–705.

Yeasmin, D. & Pasha, M. 2008 Runoff prediction by GIS using optimal number of rain gauges. In World Environmental and Water Resources Congress, Honolulu, Hawaii, 2008, pp. 1–9.

Yu, P.-S., Yang, T.-C. & Chen, S.-J. 2001 Comparison of uncertainty analysis methods for a distributed rainfall–runoff model. *J. Hydrol.* **244** (1–2), 43–59.

Zhang, X. S. & Srinivasan, R. 2009 GIS-based spatial precipitation estimation: a comparison of geostatistical approaches (1). *J. Am. Water Resour. Assoc.* **45** (4), 894–906.

Zhang, X. & Srinivasan, R. 2010 GIS-based spatial precipitation estimation using next generation radar and raingauge data. *Environ. Modell. Softw.* **25** (12), 1781–1788.